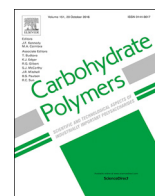




Contents lists available at ScienceDirect

## Carbohydrate Polymers

journal homepage: [www.elsevier.com/locate/carbpol](http://www.elsevier.com/locate/carbpol)

# Selective recrystallization of cellulose composite powders and microstructure creation through 3D binder jetting<sup>☆</sup>

Sonia Holland<sup>a,b</sup>, Chris Tuck<sup>b</sup>, Tim Foster<sup>a,\*</sup><sup>a</sup> Division of Food Science, Sutton Bonington Campus, University of Nottingham, Loughborough LE12 5RD, United Kingdom<sup>b</sup> 3D Printing and Additive Manufacturing Research Group, University Park, University of Nottingham, Nottingham NG7 2RD, United Kingdom

## ARTICLE INFO

## Keywords:

Cellulose  
Glucomannan  
Recrystallization  
3D Printing  
Binder jetting

## ABSTRACT

Binder jetting is an additive manufacturing technique in which powdered material is sequentially laid down and printed on by an ink binder, in a selective manner, to form a 3D object. Unfortunately work in this area relevant to food materials is largely unpublished, however a typical application of this technique is sugar powder bound by a water and alcohol based ink with optional colour or flavour demonstrated by commercial ventures. In this work we demonstrate the use of a small scale powder layering device under an ink jet printer to test prototype powders prior to producing quantities typically used in commercially available binder jetting machines. Powders comprising predominantly of ball milled, amorphous cellulose were successfully used to create 3D structures when interacting polysaccharides were present in the ink (xanthan gum) and as a proportion of the powder component (glucomannan) by inducing selective recrystallization. These ingredients are categorized as dietary fibre, thus such formulations can be used to create low-calorie 3D printed food designs to be used within food products.

## 1. Introduction

The first record of applying additive manufacturing (AM) to food materials can be found in a patent by Yang et al. (2000) describing the creation of a complex 3D cake using an extrusion based layering mechanism. Though filed in the millennium year there is no further record of such a food-specific printer being created by the inventors. In more recent years the interest in applying food materials to additive layer manufacturing techniques from businesses and researchers has boomed, evidenced by the recent Journal of Food Engineering Special Issue on 3D Food Printing (3D Printing and AM are often used as interchangeable terminology). A short time ago it was difficult to find published work on 3D printed food (Lanaro et al., 2017) but now a number of research papers, such as those from Millen, Gupta, Sen, and Archer, (2012); Derossi, Caporizzi, Azzollini, and Severini, (2017); Vancauwenberghe et al. (2017) and Sozer, Lille, Nurmela, Nordlund, and Mets, (2018), in addition to reviews from Southerland, Walters, and Huson, (2011); Wegrzyn, Golding, and Archer, (2012); Godoi, Prakash, and Bhandari, (2016); Lipton (2017) and Sun, Zhou, Yan, Huang, and Lin, (2018) are available on the topic. The majority of research papers focus on extrusion based AM with various setting

mechanisms with relatively few papers published regarding powder processes. In any case, this is indicative of a greater understanding of food materials related to different AM processes forming within the field, but there is still much more that we can learn.

As with all AM techniques powder-based AM first involves slicing a 3D computer design into 2D segments to be printed. A powdered substrate is sequentially layered in the print bed and the 3D design is constructed by binding each powder layer as the 2D slices. Binding these layers in horizontal and vertical directions may occur through thermal sintering or application of a binding 'ink'. Food specific examples include 3D sugar hot air sintering on the 'CandyFab' Printer (EvilMadScientist Laboratories: Oskay, 2007), laser sintering of Nesquik<sup>™</sup>, sugar and other powders (TNO: Sol, Van Der Linden, & Van Bommel, 2015) or binding ink-mediated sugar creations with the ChefJet Pro (3D Systems, 2018). In addition, two patents exist describing potential food-grade powder bed printing methods, with accompanying 'recipes' or formulations which may be used to create a variety of textured products (Diaz et al., 2017; Von Hasseln et al., 2014). Powders used are typically pure sugar or sugar-based, which will have implications on how they effectively bind together. These short chain carbohydrates (like sucrose) or dextrans (such as maltodextrin)

<sup>☆</sup> This work was supported by the Engineering and Physical Sciences Research Council [grant numbers EP/I033335/2, EP/K030957/1]; and a gift by the University of Nottingham.

\* Corresponding author.

E-mail address: [tim.foster@nottingham.ac.uk](mailto:tim.foster@nottingham.ac.uk) (T. Foster).

<https://doi.org/10.1016/j.carbpol.2018.07.064>

Received 7 May 2018; Received in revised form 20 July 2018; Accepted 21 July 2018

Available online 27 July 2018

0144-8617/ © 2018 The Authors. Published by Elsevier Ltd. This is an open access article under the CC BY license (<http://creativecommons.org/licenses/by/4.0/>).

are naturally ‘sticky’ materials and are often used in the food or pharmaceutical industries as binding agents, making them well suited to a binder jetting AM approach (Chumnanklang, Panyathanmaporn, Sithiseripratip, & Suwanprateeb, 2007; Cuq et al., 2013; Diaz et al., 2017). It is of interest to the food industry to look at alternative food powders for these processes as official bodies are advising consumers and producers to limit sugar intake (Public Health England, 2015) but also as a means of expanding the number of potential end-use products that could be obtained.

Cellulose, the most abundant polymer on Earth, is a building block of plant cell walls. Humans do not possess the necessary enzymes to digest it, therefore it contributes to the diet as ‘dietary fibre’ (Cui & Roberts, 2009; Wüstenberg, 2014). Cellulose is composed of  $\beta(1-4)$  diequatorially linked D-glucose molecules that associate through strong hydrogen bonding and pack together in a hierarchical fashion. Within the plant cell wall other polysaccharides are associated with cellulose, such as hemicelluloses, pectin and lignin (Gibson, 2012). It is logical, then, that researchers have found that interactive effects exist between glycans with stereochemically similar  $\beta(1-4)$  linked backbones such as galactomannans, glucomannans and the extracellular polysaccharidexanthan gum (XG) (Abbaszadeh, MacNaughtan, & Foster, 2014; Chanliaud, Burrows, Jeronimidis, & Gidley, 2002; Dea & Rees, 1987; Stephen, Phillips, & Williams, 2006; Whitney, Brigham, Darke, Reid, & Gidley, 1998). There is strong evidence for a stoichiometric factor involved in the effectiveness of these heterotypic binding interactions with the optimum ratio of  $\sim 1:1$  between co-synergist components (Abbaszadeh, MacNaughtan, Sworn, & Foster, 2016; Goycoolea, Richardson, Morris, & Gidley, 1995). The conformational state of XG as either an ordered 5-fold helix or disordered coil in its ability to participate in these interactions has been debated for some time (Abbaszadeh et al., 2016; Cairns, Miles, & Morris, 1986; Cairns, Miles, Morris, & Brownsey, 1987; Dea, Clark, & McCleary, 1986; Goycoolea, Richardson et al., 1995; Morris, Rees, Young, Walkinshaw, & Darke, 1977). Changes in ionic strength and solvent properties affect the helix-coil transition of XG. Given the presence of ethanol and modification of XG used in the present study this will be discussed briefly in the context of work presented here, however more insight will be given in an intended future publication from our research group. The abundance of cellulose in nature and potential health benefits conferred through consuming dietary fibres make it an interesting material to study as a candidate for use in a powder AM process.

By creating 3D structures based upon cellulose using an AM process we envision the possibility of mimicking assemblies relevant to food products, such as the gluten networks present in breadsticks or cookies. The printed structures could act as ingredients in a food manufacturing process by providing a crumbly or brittle textured ‘skeleton’ onto which coatings are added to enhance palatability. This could be a viable route to create low calorie snack products utilising novel and exciting technology (3D printing) for the food industry.

The previous experimentation which led to the 3D application described in the present work (Holland, Foster, MacNaughtan, & Tuck, 2018) involved formulating both a usable cellulose powder (CP) and XG based ‘ink’ component, then testing the interaction between these in a 2D scenario. The results from powder and ink characterisation plus preliminary tests in 2D could then be extrapolated into a 3D layering process with intended layer height of 100  $\mu\text{m}$ . Our previous work showed that high speed, short time mechanical attrition of cellulose reduced the particle size (from  $D[3,2] = 16$  to  $D[3,2] = 13$ ), crystallinity (from 25% to 6%) and viscosity average degree of polymerisation (from 1339 to 411) of the original sample. The native cellulose fibrillar structure was also lost, rendering a powder with semi-spherical particles of polydisperse size which was passed through a 100  $\mu\text{m}$  sieve to remove any aggregates larger than the intended layer height (see SEM images in Holland et al., 2018). Recrystallization of the amorphous powder could be achieved by imposing different moisture and temperature regimes on the sample. Therefore it was hypothesised that layer

adhesion of amorphous cellulose particles through deposition of an aqueous binder and a post-process heating step could be used to selectively induce recrystallization and create controlled structures in a binder jetting AM process. Not discussed in our previous work was the inclusion of other  $\beta(1-4)$  glycans in the powder component to evoke synergistic interactions. During the present work, it became clear that composite powders would be favourable in creating 3D structures, therefore this will be analysed in detail below.

Suitability of ink formulations was determined in terms of their ‘printability’, characterized by the Z number (Derby, 2010). Viscosity ( $\eta$ ), surface tension ( $\gamma$ ) and density ( $\rho$ ) parameters were measured for each ink to assess whether they fell within a theoretically ‘printable’ range ( $Z = 1-10$ ) out of a nozzle, whose diameter ( $L$ ) = 21  $\mu\text{m}$  by using the equation:  $Z = \frac{\sqrt{\gamma\rho L}}{\eta}$ . Inks tested attained Z numbers higher than this range, falling into the region where satellite droplets may form. Upon experimental testing in an ink jet printer it was found that the satellite droplets produced re-formed with the main droplet during flight out from the nozzle, thus not negatively impacting the printing process. Unmodified and modified XG was included in the ink formulations presented in the previous work, but at relatively low concentrations (0.25%wt). Similarly to cellulose, ball mill treatment of XG was shown to reduce its molecular weight, signified by a viscosity decrease at any given shear rate for 0.5%wt aqueous solutions. Simultaneously the ball milling increased the molecular weight distribution within the sample, shown as an elongation of the Newtonian plateau region, whilst giving similar viscosities at high shear for a given concentration of XG. The advantage of this was that the viscosity at printing shear could be maintained without the potential for long polymer chains clogging the printing nozzle. Nor would they be subject to disadvantageous molecular scission as a result of high shear rates experienced at the nozzle during printing. Additionally, a higher concentration of XG was able to be included in ink formulations, thus presenting a higher number of accessible chains which could interact with the cellulose powder. The inks with ball milled XG also attained lower Z numbers. Subsequently, given the evidence for component stoichiometric ratio to impact on synergistic interactions, further formulation of these inks has been carried out and will be detailed below.

Building on the outcomes of our previous work (summarised above), the results discussed in this paper translate findings from 2D powder-ink interaction tests into a 3D binder jetting equivalent system. In addition, interactive glycans have been incorporated into the powder component and xanthan gum loading of the ink has been increased to enhance binding and structure creation.

## 2. Experimental

### 2.1. Materials

CP used was Solka Floc 300FCC sourced from the International Fiber Corporation, USA. XG was “Grindsted Xanthan Clear 200 A21111” grade with standard acetate (6.19%)/pyruvate (3.85%) levels and provided by Danisco/DuPont Company, France. Absolute ethanol and tween 20 from Sigma Aldrich, UK were used alongside ultrapure water in the formulation of inks. Locust Bean Gum (LBG) used is available under the brand name Genu Gum type RL-200 from CPKelco (batch no: SK34260). Rheolex low molecular weight Konjac Glucomannan (KGM) was supplied by the Shimizu Chemical Corporation. C\*PharmDry™ maltodextrin (MD) DE 12–15 was sourced from Cargill.

### 2.2. Ball mill treatment of powder substrate

A Planetary Micro Mill Pulverisette 7 (Fritsch GmbH, Germany) with six 10 mm  $\Phi$  zirconium oxide ( $\text{ZrO}_2$ ) balls per 12 mL  $\text{ZrO}_2$  pot was used to mill powders. Powder weight remained at 1 g per pot and

milling was undertaken as six cycles of 5 min milling followed by 10 min pause to give 30 min total milling at 800 rpm.

Ball milled (BM) samples produced and tested in the printing scenario comprised of pure cellulose (SF300) and composite powders of cellulose with LBG or KGM in admixture prior to milling at 1:1, 7:3 and 9:1 ratios.

### 2.3. Differential scanning calorimetry

Cellulose composite powders were equilibrated over a saturated solution of MgCl<sub>2</sub> to give an atmosphere of RH 33%. Thermal transitions were monitored using a heat flux DSC 823e (Mettler Toledo, Leicester, UK) with auto sampler and liquid nitrogen cooling attachment. Samples were loaded into stainless steel pans (Perkin Elmer), hermetically sealed and run from –40 °C to 150 °C with a scan rate of 10 °C min<sup>-1</sup> with a subsequent cooling at 50 °C min<sup>-1</sup> and holding time for 5 min at –40 °C then a reheat step.

A Setaram MicroDSC III calorimeter (SETARAM, France) was used to observe changes to ordering and disordering transitions of XG solutions upon application of thermal energy as a result of ball milling. With water as a reference, ≈800 mg of sample was loaded into the sample cell at 20 °C then cooled to 10 °C. A temperature ramp to 95 °C and back to 10 °C at 1 °C min<sup>-1</sup> was conducted twice on the sample and data taken from the second scan to ensure the samples had the same thermal history.

### 2.4. Ball mill treatment of xanthan gum

The equipment set up was identical to section 3.2. However, due to the smaller starting particle size of XG, 3 g of powder was added per pot to retain the desired fill volume. In addition to those outlined in the previous work a further milling cycle of 120 min at 800 rpm was introduced to give four potential XG samples to use in ink formulations: Native, 400 rpm 60 min, 800 rpm 60 min and 800 rpm 120 min.

### 2.5. Ink formulation and characterisation

1%wt and 2%wt XG stock solutions were created through dissolution of each sample in ultrapure water, whilst stirring, then heating this solution to 85 °C for 30 min to allow full polymer dissolution. Solutions were cooled, transferred to a tube roller at 4 °C for 12 h and stored at 4 °C until use. Ethanol, Tween 20 and additional water were added to stock solutions in necessary amounts to create the ink formulations presented below in Table 1.

#### 2.5.1. Viscosity of XG stock solutions and ink formulations

Flow curves were developed using a MCR301 rheometer (Anton Paar, Austria) with double gap geometry. Shear rate was varied logarithmically from 0.1 to 1000 s<sup>-1</sup> with 7 measuring points per decade, measurement time intervals were varied initially set to 10 s and ending at 1 s. The system was kept at 30 °C throughout with 2 min equilibration time allowed prior to shearing. Samples were measured in triplicate and 100 cSt silicone oil (Dow Corning, USA) used as a standard prior to measurements on different days

**Table 1**

Ink formulations tested for printing in this work. The nomenclature for ‘formulation’ gives the concentration of XG (%wt), ball milling speed (rpm) and ball milling time (min). Measured parameters and calculated Z value for each ink formulation are also given, differing letters (a, b, c) denote significantly different values  $p < 0.05$  according to Tukey pairwise comparison test.

Formulation	Water (wt %)	Ethanol (wt%)	Tween 20 (wt %)	Xanthan (wt%)	Density (g cm <sup>-3</sup> )	Surface Tension (mN m <sup>-1</sup> )	Viscosity, 30 °C at 1000 s <sup>-1</sup> (mPa.s)	Z
0.25 % BM 400,60	79.25	20	0.5	0.25	0.97 ± 5x10 <sup>-6</sup> a	34.9 ± 0.8 <sup>a</sup>	1.8 ± 0.04 <sup>a</sup>	15 <sup>a</sup>
0.75 % BM 800,60	78.75	20	0.5	0.75	0.97 ± 7x10 <sup>-7</sup> b	35.0 ± 1.1 <sup>a</sup>	1.9 ± 0.005 <sup>b</sup>	14 <sup>b</sup>
1 % BM 800,120	78.5	20	0.5	1	0.97 ± 5x10 <sup>-6</sup> c	37.6 ± 0.6 <sup>b</sup>	1.9 ± 0.008b	15 <sup>a</sup>

#### 2.5.2. Surface tension of ink formulations

Drop shape analysis and surface tension were measured via the pendant drop method using a Drop Shape Analyser DSA100S (Krüss GmbH, Germany). Once the droplet profile was extracted the software calculated a surface tension value using the Young–Laplace equation. Pure water was used as a standard prior to each set of measurements.

#### 2.5.3. Density measurement

Density was determined using a density and sound velocity meter, DSA 5000 M (Anton Paar, Austria). Samples were introduced to the oscillating U-Tube with a syringe. The density was measured in triplicate, a new aliquot was then introduced and measured in triplicate again. Pure water was used to calibrate the machine prior to each use.

### 2.6. Printing equipment

#### 2.6.1. Dimatix Ink jet printer

The Dimatix DMP-2831 and cartridges with 21 µm diameter nozzles (FujiFilm, USA) were used to conduct ink jet printing. A waveform designed specifically for low viscosity inks was selected as the most ideal waveform for all inks tested. The drop watcher software function was used to assess stability and repeatability of droplets during printing.

#### 2.6.2. 2D and 3D capability

Two bespoke powder substrate holders were designed for use in the Dimatix printer. The first allows powder and ink compatibility testing in 2D (single layer printing) and determination of the required ink : powder saturation due to the inclusion of 100–400 µm deep indents.

The second enabled printing in 3D (multi-layer printing). A holder was designed in CAD and laser sintered using Polyamide 12. The internal section housed magnets and acted as the print bed whereas the outside border was used to collect excess powder after layer spreading. Aluminium Shims 100 µm thick were cut to create basic 40 x 20 mm frames. These frames were stacked one by one on the magnetic centre (process 1) with powder spread across the gap with the long edge of a glass microscope slide (process 2) and selected areas printed on in between (process 3), thus creating a 3D system with 100 µm layers. The magnetic base enabled accurate superimposition of subsequent layers and prevented movement of each metal layer during the spreading process. The 2D recessed plate, an annotated diagram of the 3D set up and schematic of the printing process can be seen below in Fig. 1. After the printing and layering process was complete, the whole system was placed in a convection oven to deliver the thermal energy required for recrystallization of ink-saturated powder. The 3D object was removed from the surrounding unbound powder with tweezers.

### 2.7. Wide angle X-Ray diffraction (WAXD)

To validate the success of selective recrystallization during the 3D process a Bruker D5005 Diffractometer (Bruker AXS, UK) was used to observe the diffraction patterns of both printed products and the surrounding unbound powder with Copper K alpha (CuKa) radiation of wavelength 1.5418 Å. Data collected was within the angular range 2θ 3–38° at 0.05° increment step. Subsequent crystallinity calculation was

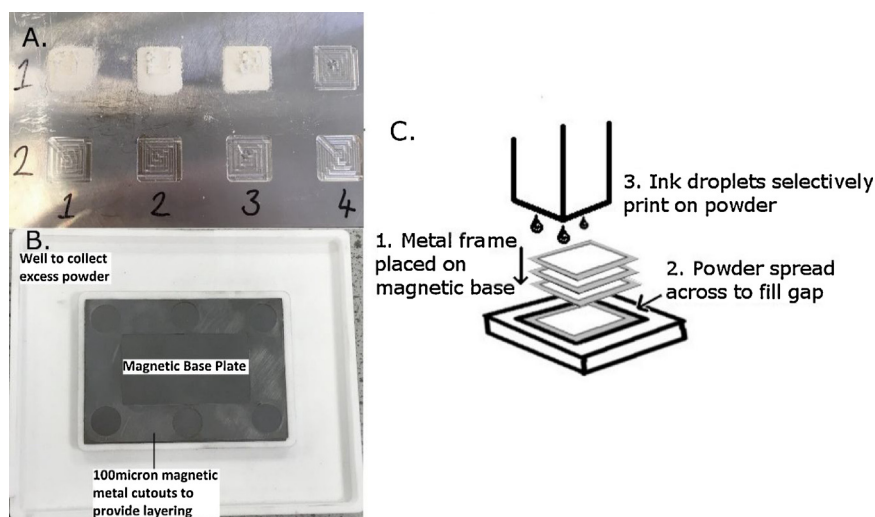


**Fig. 1.** A. 2D recessed plate for testing powder and ink interaction; B. 3D powder layering mechanism, to be situated on the Dimatix printer platen for the duration of printing with the addition of one metal sheet per layer of powder and ink; C. Schematic of experimental 3D layering system in use with processes 1, 2 and 3 repeated until the final ink layer has been printed.

conducted on Microsoft Excel software using the curve fitting approach based on Paes et al. (2010) and Winkworth-Smith (2014).

### 2.8. Scanning Electron Microscopy (SEM)

A Hitachi TM3000 Table Top SEM (Hitachi High Technologies, USA) was used for printed sample visualisation. Samples were mounted on 12.5 mm  $\Phi$  stubs with carbon tape before being platinum coated using an Emitech SC6740 Sputter Coater (Polaron Ltd, UK).

### 2.9. X-ray Micro computed tomography (MicroCT)

Samples were mounted on plastic rods using epoxy resin and scanned in 3D using the GE Phoenix Nanotom 180NF (GE, Germany) X-ray Computed Tomography System. The scan consisted of collecting 1200 projection images over 360° at an electron acceleration energy of 50 kV and a current of 240  $\mu$ A. Each projection image was the average of three images (to reduce image noise) using a detector timing of 500 ms, resulting in a total scan time of 1800secs (30 min). The sample spatial resolution varied from 1.25 to 1.5  $\mu$ m/voxel depending on sample. Data was visualised and prepared for analysis using VGSTUDIO MAX V.2.2 Software (Volume Graphics, Germany). A median filter was used to reduce image noise, then regions of interest (ROIs) were created and reconstructions rendered in 3D.

#### 2.9.1. Image analysis and data processing

Fiji, an open source image processing package by ImageJ (see Schindelin et al., 2012), was used to analyse stacks of 2D images. Three stacks of 200 images each were selected from different regions running through the 3D object. Each stack underwent a thresholding step to create a binary image and both light and dark noise below 3x scan resolution was removed from the images. ROIs were selected running through a given stack so that the area being analysed always contained particles and was not on the periphery of the object.

When processing images for the maltodextrin sample the air bubbles and crack features were analysed using the 'Analyse Particles' ImageJ plugin, whereas for the cellulose sample the LUT was inverted after thresholding to allow analysis of the particles. Computed values for average size and percentage area were not significantly different between regions of interest (ROIs) and stacks for either sample. ImageJ also allows analysis of particle aspect ratio and average roundness  $4 \frac{\text{Area}}{\pi [\text{Major Axis}]^2}$  with 1 being a perfect sphere and 0 an infinitely elongated polygon (ImageJ User Guide, Rasband, 2018).

Statistical analysis was undertaken in Minitab® 17.2.1 (UK). Within each stack for any given parameter 200 values per ROI were available,

these were averaged to encompass all variability for a measurement, resulting in three or four values per stack of 200. These values were then subjected to ANOVA to determine whether statistically significant differences could be seen depending on the image stack location within the printed object.

## 3. Results and discussion

### 3.1. Further ink formulation

Ball milling of XG at 800 rpm for an extended period of time (120 min) produced a sample that, when in solution at 0.5%wt, exhibited a much longer zero-shear plateau before a less extreme shear thinning region was observed at shear rates higher than 10  $\text{s}^{-1}$ . In Fig. 2 this can be compared to the relatively short zero-shear plateau of native XG at equivalent concentration. However at high shear rates, relevant to ink jet printing, the solution viscosity at 0.5%wt is very low. This is actually advantageous, as increasing the solution concentration to 1% wt XG a printable ink viscosity is maintained whilst allowing a higher effective concentration of XG to be available for interaction with the polysaccharides in the powder constituent. As discussed in the previous work, ball mill treatment of XG lowered the sample molecular weight, indicated by a solution viscosity decrease at a given concentration. Ball milling for 60 min at both 800 rpm and 400 rpm in the previous work showed little change to the viscosity at high shear for 0.5%wt solutions compared with native XG. Using the higher of these speeds and doubling the milling time, tested in the current work, has had a much greater effect which will be discussed below. Lower molecular weight polymers are less likely to cause nozzle blockage compared with the native high molecular weight, long chain polymer. The zero shear plateau also becomes longer for samples ball milled for a longer time or at a higher speed, indicative of a wider molecular weight distribution. This is expected, considering the non-specific destructive nature of the ball milling process and equivalent results observed for other polymers, such as cellulose.

The 0.5%wt solution of XG ball milled at 800 rpm for 120 min was printable without adding ethanol and Tween 20, but droplet formation was not consistent. With added water, ethanol and tween 20 1%wt of the newly milled XG could be incorporated into the ink whilst maintaining the appropriate printing characteristics. Therefore, through milling, a higher weight percentage of XG could be incorporated into the ink, increasing the interaction with the cellulose powder substrate as described above. The range of flow curves (A) in Fig. 2 show how modulation and tailoring of ink formulation flow properties can be achieved through the addition of mechanically modified XG. Ethanol is

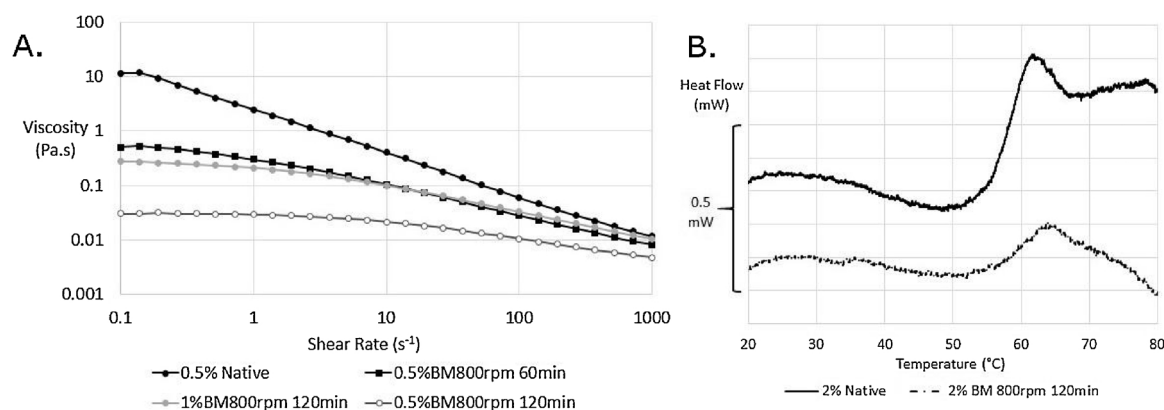


**Fig. 2.** The effect of ball milling on XG properties. A: Flow curves of a 0.5% native XG solution versus those at 0.5% and 1% of XG milled at 800 rpm for 120 min, alongside the 800 rpm for 60 min BM sample presented in [Holland et al., 2018](#) for comparison. B: Enthalpy on cooling of 2% solutions of native XG and BM XG 800 rpm, 120 min. The modified XG solutions presented here have been used in ink formulations.

a low viscosity, low surface tension substance which is miscible with water. It is often used as a co-solvent in edible and non-edible aqueous ink formulations for its favourable properties ([Pallottino et al., 2016](#); [Kipphan, 2001](#)). At 20%wt the solvent volatility should not cause excessive drying at the nozzle, nor precipitate XG from solution ([Garcia-Ochoa, Santos, Casas, & Gomez, 2000](#)). Further information on the effect of ethanol on XG in solution will be presented in another paper from our research group, currently in progress. [Fig. 2 B](#) shows the exotherms upon cooling of 2% XG solutions of native and the most intensely ball milled samples obtained via microcalorimetry. The lowering of intensity of the coil-helix ordering transition occurring between 65–50 °C as well as reduction in peak sharpness and slope gradient are evident. This indicates that the ball milling process is affecting the ability of XG molecules to form helices in solution. The proposed mechanism for this effect is that the reduction in molecular weight is sufficient to drop below the required critical chain length for helix formation and association in some instances, a phenomenon seen with other polymers ([Aymard et al., 2001](#)) as well as XG with respect to solvation in molecular dynamic simulation studies ([Ong, O’Byrne, & Liow, 2018](#)). Due to the larger molecular weight distribution and lower average molecular weight observed through rheological studies it is likely some of the sample has been broken down to this extent during the intense milling regime. The material that survives milling forms helices at the same temperature as the unmilled samples, which indicates that the milling process itself does not change the chemical composition of XG (i.e. acetate and pyruvate content), as this is known to shift the thermal transitions.

### 3.2. Selective recrystallization in 3D

The ability to recrystallize dissolved cellulose is well documented and is utilised in industry to create fabric fibres ([Klemm, Schmauder, & Heinze, 2002](#); [Rosenau, Potthast, Sixta, & Kosma, 2001](#); [Wüstenberg, 2014](#)). Cellulose treatments such as mercerization (alkali treatment with NaOH) and the Lyocell process, which uses *N*-methyl morpholine-*N*-oxide (NMMO) solvent, involve recrystallization to cellulose type II upon, solvent exchange with polar solvents, which is more thermodynamically stable (with adjacent cellulose chains anti-parallel to one another) than the type I, natural form of cellulose ([Burrow, 2005](#); [Goda & Sreekala, 2006](#); [Klemm et al., 2002](#); [Rosenau et al., 2001](#); [Wüstenberg, 2014](#)). A number of studies have also researched the recrystallization of ‘amorphous’ cellulose produced via ball milling. Though [Hermans and Weidinger \(1946\)](#) concluded differently, [Hess, Kiessig, and Gunderman, \(1941\)](#); [Paes et al. \(2010\)](#); [Hajji, Mitchell, and Foster, \(2011\)](#), and [Winkworth-Smith \(2014\)](#) found that the ball milling time had an influence on the ratio of type I : type II crystal allomorphs present in a given recrystallized sample, independent of the initial

cellulose source used. Regardless, recrystallization was always performed on the entirety of a sample either through equilibration at selected relative humidities or drying with or without first saturating with an anti-solvent.

We previously described the production of an amorphous cellulose powder by ball mill treatment and defined a moisture and temperature dependency on its recrystallization with thermal analysis after equilibration over selected saturated salt solutions. It was concluded that extrapolation of this knowledge into a binder jetting scenario would lead to the selective recrystallization of powder printed on with the ink, leaving the surrounding unbound powder in an amorphous state as is detailed in the results obtained below.

Using the standard ball milled cellulose powder and both ink 0.25% BM400 rpm, 60 min and 1%BM800 rpm, 120 min 10 x 10 mm 3D square blocks were created of various heights using the 3D set up described in section 3.6.2. Preliminary testing revealed that the perimeter of an ink droplet on a model porous substrate was slightly larger than the nozzle diameter of 21 μm (results not shown). To ensure a good overlap of droplets and sufficient saturation of powder a 10 μm spacing was selected for printing. This drop spacing equates to 2540 drops per inch (DPI). Ideally, through use of a binder jet system with a heated bed capacity, the bulk powder would be kept a few degrees below the target recrystallization temperature (determined on relating thermal properties of the particular powder composition to the ink : powder saturation ratio) and recrystallization would be ‘instantaneous’ as the ink is jetted onto the substrate. However for the proof of principle set up used here this was not possible. Instead, the entire system was placed in an oven after printing and layering had been completed to provide the necessary heat for recrystallization. The printed structure and surrounding unbound powder were collected separately and analysed with WAXD. From [Fig. 3](#) it is clear that the powder which had been printed on had partially recrystallized whereas the bulk powder surrounding it had not, despite both phases being subjected to the same heat treatment for the same time. The amorphous powder remaining could be collected and re-used in such a process, with automation, thus allowing structure development without material wastage.

The crystallinity values determined from peak deconvolution indicated that the resulting partially crystalline sample had a mixture of type I and type II cellulose (see [Table 2](#) below). Visually, this is apparent by the sample tendency to recrystallize with a more dominant peak between 2θ 21–22°, in line with the 200 Miller Index which is usually at its maximum at 21–23° ([Ghaffar, 2016](#)), and the 040 peak just below 35° re-emerging as a sign of cellulose I<sub>β</sub> crystallites ([Ju, Bowden, Brown, & Zhang, 2015](#); [Park, Baker, Himmel, Parilla, & Johnson, 2010](#)). This result is expected as more recent studies on ball milling and recrystallization of cellulose, mentioned above, suggest that with longer milling times recrystallization to type II is favoured, whereas type I (or

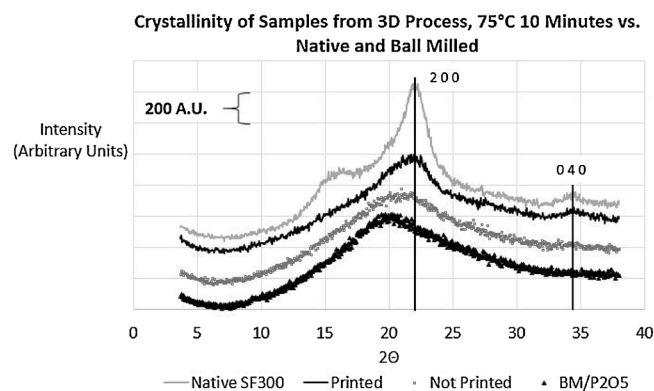


**Fig. 3.** WAXD of native cellulose (top) which has been ball milled and stored over a desiccant, P<sub>2</sub>O<sub>5</sub>, (bottom) and the powder which has undergone selective recrystallization by being printed on or not (middle). Lines highlight two key Miller Indices relating to crystallographic planes of cellulose particularly relevant for crystallite size, paracrystalline cellulose levels and packing efficiency of chains.

**Table 2**

Crystallinity of cellulose only and mixed powder systems after printing and recrystallization.

Powder Formulation	Crystallinity (%)		
	Total	Type I	Type II
BM Cellulose	17.17	7.96	9.21
9:1 BM Cellulose/LBG	17.21	7.81	9.4
9:1 BM Cellulose/KGM	19.31	10.74	8.57

a mixture) is favoured for short to medium milling times. The milling regime of 800 rpm for 30 min produces a sample on what the authors refer to as the ‘amorphous threshold’ i.e. this was the first time period at the given rpm that the diffraction pattern exhibited a broad, featureless Gaussian-like shape indicative of a sample lacking in order. Deconvolution of this indicated that a small amount of residual type I crystals were present in the milled sample. Thus on recrystallization during the printing and heating process it is likely that these contributed a ‘seeding’ effect for more type I crystal propagation. In localised areas of the sample where these seeds were not present (which could be truly described as ‘amorphous’ regions) the more thermodynamically stable type II crystal lattice would be favoured.

A range of temperature and time combinations were tested to ascertain which allowed sufficient heat transfer through the powder bulk. It was found that 10 min in an oven set to 75 °C achieved the desired selective recrystallization of powder which had been printed on without causing detrimental effects, such as surface cracking, that occurred at heat treatment of higher temperature/shorter time.

### 3.3. Effect and concentration of additional powder components

Structures comprising of pure cellulose were very brittle and difficult to handle, even though they had partially recrystallized. Solid objects such as the squares described above in section 4.2 could be removed easily from the powder bed but more complex designs were less successful. As discussed in the introductory section other stereochemically similar polysaccharides are known to interact with cellulose, including galactomannans (e.g. LBG) and glucomannans (e.g. KGM). The DSC traces in Fig. 4 confirm changes to the thermal behaviour of such mixtures with the system recrystallization event highlighted by an arrow. The other peak observed at ~ 50–60 °C relates to a generic polymer relaxation peak, described by Appelqvist, Cooke, Gidley, and Lane, (1993). This transition is seen for a broad range of polymers; its enthalpy but not temperature position is affected by water content of

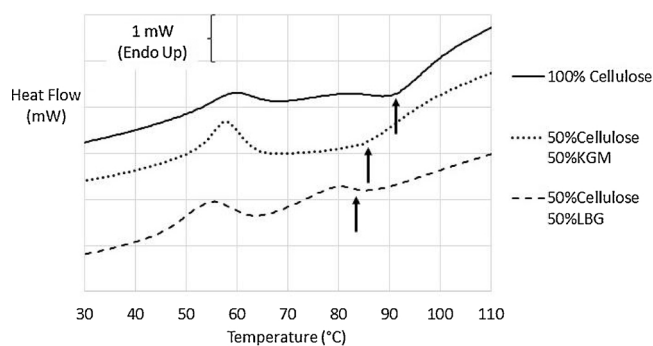


**Fig. 4.** DSC of powders equilibrated at 33%RH. Arrows indicate the lowering of transition temperatures with varying powder composition.

the sample.

Initially 1:1 admixtures of cellulose with LBG and KGM were ball milled as described in section 3.2. When tested in the 2D recessed plate with all ink formulations the resulting films were noticeably porous, rather than cohesive, and had a tendency to ‘lift’ from the powder surface, rather than absorbing ink in a uniform manner, to create warped films. Translated to a 3D process this is a major issue as layering more powder on top would disturb the printed pattern underneath, causing misalignment and destroying the intended 3D structure. Both LBG and KGM are hydrophilic polymers. As ball milling is both a destructive and non-selective process the molecules are randomly broken up. This may expose reactive groups which may not ordinarily be available by disrupting ordered molecular conformations and hyperentanglements (detailed below). As mentioned in the introductory remarks, an optimal 1:1 ratio was identified for β(1–4) glycan synergistic interactions (Goycoolea, Richardson et al., 1995). This stoichiometric relationship has not specifically been discussed in literature for galactomannans or glucomannans with cellulose, but there is strong evidence that this is the case (Abbaszadeh et al., 2014). As the printed systems contain ball milled fragments of cellulose, XG and either LBG or KGM there are a number of possible mechanisms to consider. Certainly there is a physical effect of heterogeneous moisture loss and drying within the cellulose/LBG samples and to a lesser extent cellulose/KGM samples, which is not apparent within the cellulose only sample (see Fig. 5). Warping in 3D binder jetting is a known issue typically caused by delayed solidification and in-homogenous shrinkage during printing (Schmutzler, Zimmermann, & Zaeh, 2016). Within the system presented here this could be explained by a preference of ink moisture absorption by the hydrophilic LBG and KGM fragments present within the sample compared with cellulose fragments. Thus moisture distribution in the sample would not be homogenous and directly affect drying kinetics. This, however, would imply competition rather than synergism between the polymers present. What is more likely, given information available in literature and the observed impact of LBG and KGM on the

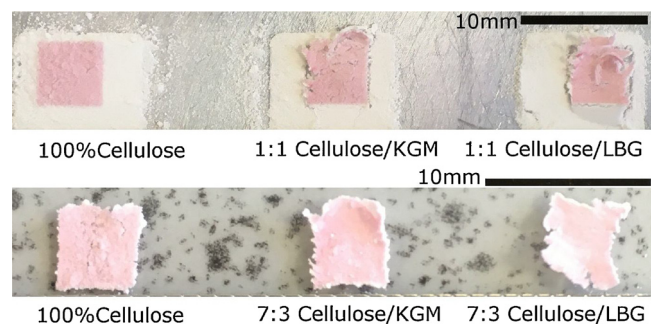


**Fig. 5.** Squares right to left: pure BM cellulose, admixture with KGM and admixture with LBG. Top: 50% cellulose, 50% KGM or LBG. Bottom 70% cellulose, 30% KGM or LBG.

cellulose recrystallization transition in Fig. 4, is that the synergistic molecular interaction of components is greatest at this 1:1 ratio but macroscopically this does not translate to linear effects. Molecular re-ordering and heterogeneous moisture release on drying during recrystallization, as well as film formation of dried gel through specific interactions of XG with LBG or KGM, cause warping at the corners of single layer printed squares. What is evident in Fig. 5 is that increasing the relative content of cellulose in the powder compared with LBG and KGM slightly mitigates this negative warping effect (a ‘failure’ for translation to 3D) whilst also giving enhanced single layer cohesion in 2D printing. Therefore the cellulose fraction in admixture was further increased relative to the LBG and KGM sequentially, with the most promising results being observed with 9 parts cellulose to 1 part added polymer. 3D 10 x 10 mm squares were successfully printed with pure cellulose and 9:1 ball milled mixtures of cellulose and LBG or KGM. The crystallinity profiles are compared with that of a printed 100% cellulose sample in Table 2.

Though XG acts synergistically with both LBG and KGM, the synergism is greater for glucomannans due to the higher proportion of unsubstituted sections of the glucomannan backbone (Stephen et al., 2006). Even with the reduced LBG fraction the powders exhibited undesirable properties for 3D structure creation such as lack of cohesion and warping (see Fig. 6), thus more complex structures in 3D were created with the 9:1 cellulose KGM ball milled powder, shown in the following section.

A possible explanation for the warping of structures containing LBG but not KGM relates to the differing chemical structures of the polysaccharides. Intermittent galactose moieties are present along the mannan backbone of LBG. In an ordered conformation, the galactose side chains prevent close association of the mannan backbones of adjacent chains in the *b* direction (Doyle, Lyons, & Morris, 2009). There is evidence of localised interactions between neighbouring galactomannan chains above a critical coil overlap concentration, termed “hyperentanglement” (Goycoolea, Morris, & Gidley, 1995). These hyperentanglements are not restricted to unsubstituted regions of the mannan backbone, along the axes of the *a* crystal lattice plane, and can occur along regions with galactose residues to create stable associations over time (Doyle et al., 2009). Cellulose chains pack together along the *b* axis to form crystalline, ordered regions (Wüstenberg, 2014). Therefore, the destructive nature of a high speed short time ball milling regime is likely to disentangle some hyperentanglements as well as breaking up the cellulose crystalline lattice, whilst leaving some type I crystal seeds as previously discussed. Upon application of the ink molecular mobility increases and this is further enhanced by the post-process heating step required to induce recrystallization. During the printing and heating processes the kinetics of recrystallization onto the type I seed templates will compete with the thermodynamic drive of fully amorphous cellulose segments to recrystallize in a type II crystal lattice structure (evidenced by the mixed lattice structures of the resulting printed objects). In amongst this, reformation of hyperentanglements between LBG fragments and their incorporation into the semi-crystalline cellulose lattice will increase spacing between chains along the *b* axis. Therefore it is unlikely that the resulting crystal structure is able to form linearly and that steric hindrance by LBG will cause directional changes and kinks on a molecular level which appear as warping on a macroscopic level. KGM, on the other hand, is unbranched and contains diequatorially linked glucose along with



Fig. 6. Warping of 3D printed 9:1 cellulose LBG powder.

mannose in the backbone, which enhances its interaction with cellulose (Abbaszadeh et al., 2014). Low molecular weight KGM (such as that used in this work) has been shown to crystallize readily into the anti-parallel mannan I lattice and interact with cellulose (Chanzy, Dubé, & Marchessault, 1978; Chanzy, Grosrenaud, Joseleau, Dubé, & Marchessault, 1982). Therefore as recrystallization ensues in this system steric hindrance will not inhibit chain packing along the *b* axis, mannan I KGM will certainly interact with the type I lattice formed through the seeding effect and perhaps also with the thermodynamically favourable type II lattice due to the antiparallel nature of chains in this configuration.

### 3.4. Creating and characterising 3D structures

As the powder layering process in this work (see section 3.6.2) was designed as a low volume, experimental set up, with a heavily manual emphasis on its ability to function, maltodextrin (MD) was used as a model powder to determine the capability of the system. The manufacturer lists relevant material applications such as excellent binding and diluent properties during compression and a suitable carrier in spray drying, thus it was a suitable model material choice.

In 2D, patterns were created as a series of individual drops facilitated by a pattern editing function in the Dimatix software. To move to 3D more complex bitmap files were imported for printing, such as star shapes to observe the resolution of sharp corners. MATLAB script was also used to create two different series of bitmap images which could be alternately printed as layers to build designs. The first script coded for two square images; one larger with a defined border thickness and hollow centre, the other a set of four solid squares whose sides were of equal length to the thickness of the border which could be used as struts on top of the larger square (A in Fig. 7). This enabled the two images to perfectly superimpose and create hollow boxes or ‘lattice’ type structures when multiple layers of each were printed. The second script coded for a series of 10 circles whose diameter decreased by one unit per time. These could be printed in sequence to produce a variety of circular based structures such as spheres, round bottomed ‘pyramids’ or ‘spinning top’ type structures (B in Fig. 7). Length scales are not specifically mentioned in the descriptions as these could be changed in the script, depending on the desired size of the final structure.

In Fig. 8 printed pieces made entirely of MD are shown, including an SEM micrograph of the surface and internal structure, visible by fracturing the sample prior to Pt coating.

Fig. 9 shows successfully printed square, star and ‘spinning top’ 3D pieces, and SEM of their microstructure, using 9:1 cellulose/KGM ball milled powder and an ink formulation containing 1%wt milled XG 800 rpm 120 min. More complex designs with thin ‘struts’ holding square boxes were not successfully printed without also incorporating maltodextrin into the design, for example alternately layering the cellulose and KGM powder with MD powder. In addition to confirmation

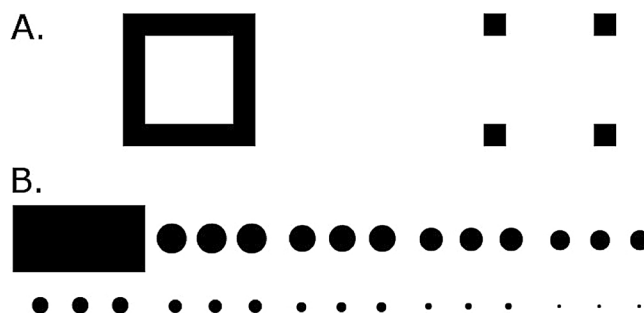


Fig. 7. A. Output of the first MATLAB script which coded for a square base and superimposed ‘struts’ to form lattice structures. B Output of the second MATLAB script which coded for a series of circles with increasingly small diameter, used to create circular based ‘pyramids’ or ‘spinning top’ type structures.

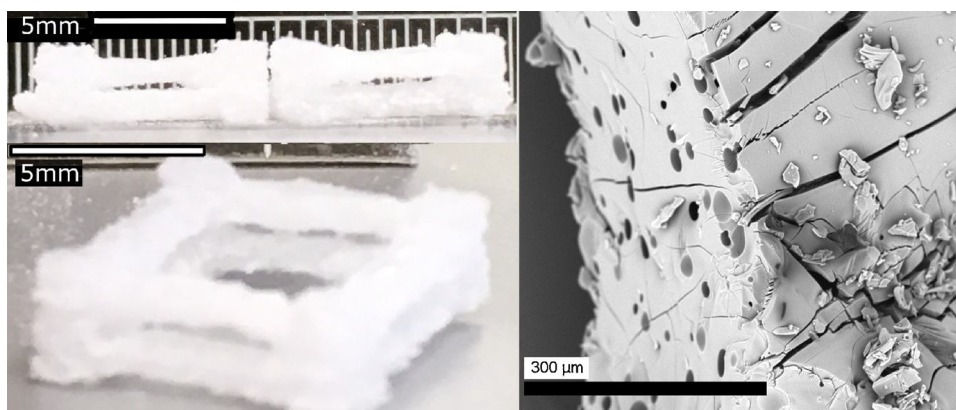


Fig. 8. Maltodextrin printed lattice structure (left) with corresponding SEM (right).

of recrystallization by XRD (section 4.2) DSC of these printed samples (results not shown) still exhibited the generic polymer peak (described by Appelqvist et al., 1993) but no longer showed the recrystallization event highlighted by arrows in Fig. 4, thus indicating that this had occurred during the printing and heating process as intended.

Scans of the printed pieces using MicroCT correlated SEM with respect to structural observations. The smooth interior, cracks, bubbles and comparatively rough exterior of the printed MD seen in Fig. 8 is also apparent in image A of Fig. 10. Similarly, the needle-like particulates contributing to a highly porous structure, seen in the top images of Fig. 9, is observable throughout the structure in images B and C of Fig. 10.

Observation of the 3D renders and stacks of 2D images acquired from MicroCT show that there is a clear difference in what may be regarded as the ‘continuous’ phase (comprising the most phase volume in the structure). For the sample made with MD powder the structure has a higher phase volume attributed to maltodextrin rather than air. The powder readily reacted with the ink via a wetting and agglomeration mechanism (Cuq et al., 2013). It is possible that this occurred to

the extent of partial or full solubilisation with subsequent hardening, as individual particles are no longer visible in these samples. Instead, heterogeneous air bubbles and cracks can be seen to be distributed throughout the structure. This behaviour can be attributed to the agglomeration binding mechanism employed by MD due to its stickiness. The air bubbles contribute to 13% of the internal area and have an average area  $460 \mu\text{m}^2$ . Conversely, the sample created from powder predominantly comprising of cellulose exhibits a much more porous, open structure of which the pore space has a larger phase volume than the printed powder. KGM is a water soluble polysaccharide which exhibits some ‘sticky’ binding effects, and is present in the powder formulation at 10%wt. However, as XRD analysis in section 4.2 shows, the main binding mechanism for this powder is through recrystallization of mechanically amorphised cellulose interacting with the KGM and XG components. A vastly different internal structure is predicted based upon this fundamental difference in binding. The counted particles make up 29% of the internal volume and have an average area  $958 \mu\text{m}^2$ . The average aspect ratio for particles within the cellulose structure was 2, however measured values varied greatly with the maximum being

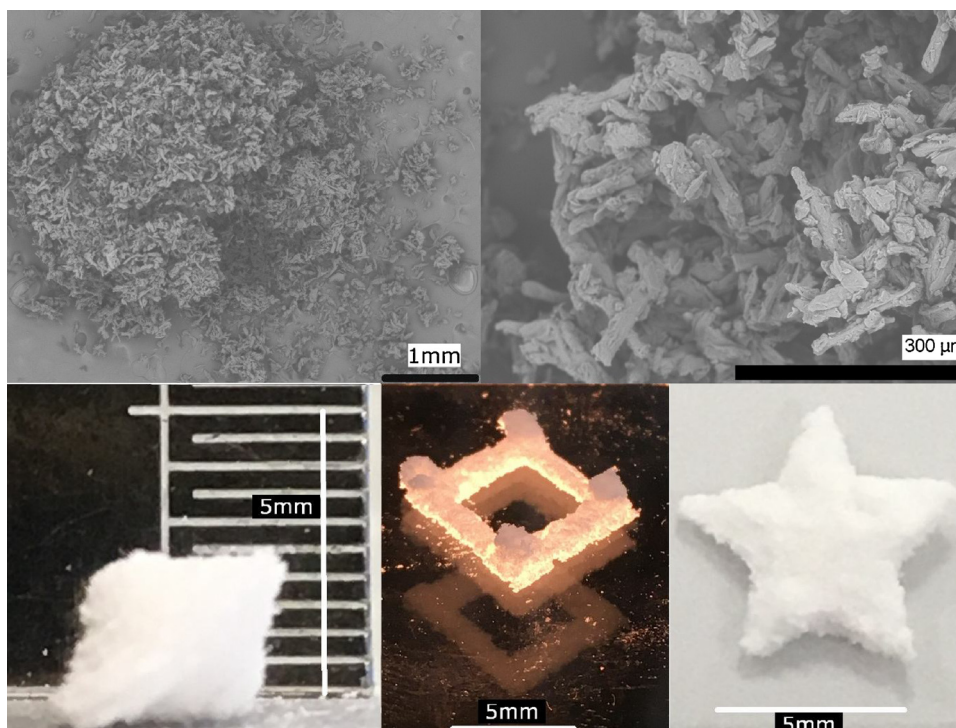


Fig. 9. Top: SEM of a spinning top at x30 magnification (left) and x250 magnification (right) of 9:1 BM cellulose/KGM. Bottom: Printed pieces made from ball milled cellulose/KGM powders. Spinning top (left), lattice (middle) and star (right).



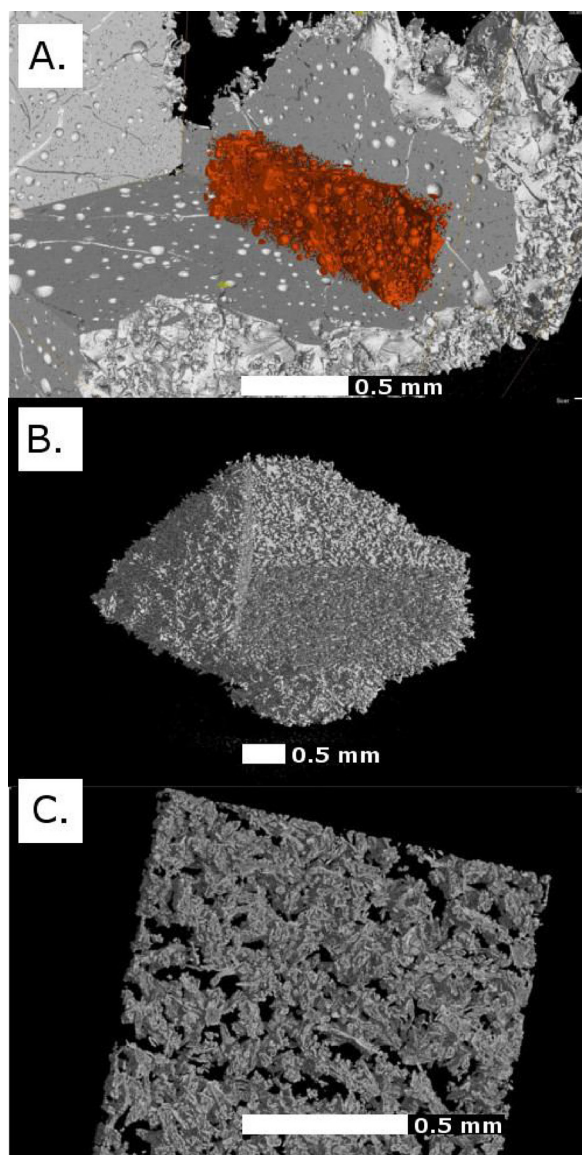


Fig. 10. A: 3D render of a maltodextrin lattice corner. Some bubbles and cracks have been individually highlighted in orange and shown as a cut out of the main structure. B and C: Whole cellulose/KGM spinning top (scanned with 6  $\mu\text{m}$  resolution) versus a region of interest from the central portion of the spinning top scanned individually at 1.25  $\mu\text{m}$  resolution.

18. Similarly, average roundness for this sample was 0.55. SEM of ball milled powders (see Holland et al., 2018) show that native particle morphology is semi-spherical, but not high aspect ratio like native, crystalline cellulose particles. In Fig. 10 the selected ROI appears to be comprised, in part, of particles with a higher aspect ratio which may be a result of the selective recrystallization event occurring during the post-print heating step.

#### 4. Conclusions

The hypothesis presented in Holland et al. (2018) that a binder jetting, AM layering technique could be utilised to provide selective recrystallization of ball milled cellulose facilitating the production of 3D structures has been confirmed. Though solid, filled structures (such as squares) could be printed with cellulose alone, the structure cohesiveness and intricacy of structures that were possible was greatly enhanced by the addition of konjac glucomannan. This is due to the synergistic effect between the three polymers used resulting from

stereochemical similarities in their backbone; cellulose, xanthan gum and glucomannan. The recrystallized cellulose structures obtained comprised of a mixture of type I and type II celluloses due to the persistence of type I crystallite seeds in the ball milled starting material. It was confirmed that only powder which had been printed on was recrystallized upon heating, the surrounding unbound powder could be collected and reused to create a no waste, sustainable system. Ball milling of xanthan gum enabled higher concentrations to be incorporated into inks whilst maintaining acceptable printing qualities. This processing of xanthan lowered the intensity of the coil to helix transition but not the temperature range over which it occurs, therefore the milling was not so severe that the chemical structure was altered. 3D structures were successfully created ranging from simple square designs to more complex stars and ‘spinning top’ geometries using a bespoke manual layering substrate system. These samples were highly porous but were still able to be handled, transported and analysed by various methods. A small scale layering system was produced and shown to be useful in testing experimental powders, allowing for flexibility in that large quantities were not required. Texture analysis of these printed materials in the future would give further insight into the product hardness and breakdown profile of the structures in relation to intended food analogues. The next stage would be to test these experimental powders in a commercial, automated binder jetting machine which would allow for a controllable powder bed temperature as well as powder spreading and layering less subject to human error than the experimental rig presented here. 3D printed designs could range from recreation of natural food structures, such as strong, brittle gluten matrices in breadsticks or cookies to mimicking porous, hard materials in the biomedical sphere and other industries.

#### Acknowledgements

This work was supported by the Engineering and Physical Sciences Research Council [grant number EP/I033335/2, EP/K030957/1] The authors would like to thank Mark Hardy, Mark East and Joseph White for their assistance in the development of 2D and 3D capabilities for the Dimatix printer, Craig Sturgess for his support in developing MATLAB scripts for 3D pattern creation and Craig Sturrock for supporting the MicroCT scanning. All MicroCT scanning was conducted at The Hounsfield Facility, School of Biosciences, University of Nottingham which received funding from the European Research Council (Futureroots Project) and The Wolfson Foundation.

#### References

- 3D Systems. Culinary 3D Printing. [online] Available at: <https://uk.3dsystems.com/culinary> [Accessed: 11 August 2015].
- Abbaszadeh, A., Macnaughtan, W., & Foster, T. J. (2014). The effect of ball milling and rehydration on powdered mixtures of hydrocolloids. *Carbohydrate Polymers*, *102*, 978–985.
- Abbaszadeh, A., Macnaughtan, W., Sworn, G., & Foster, T. J. (2016). New insights into xanthan synergistic interactions with konjac glucomannan: A novel interaction mechanism proposal. *Carbohydrate Polymers*, *144*, 168–177. <https://doi.org/10.1016/j.carbpol.2016.02.026>.
- Appelqvist, I. A. M., Cooke, D., Gidley, M. J., & Lane, S. J. (1993). Thermal properties of polysaccharides at low moisture: 1-An endothermic melting process and water-carbohydrate interactions. *Carbohydrate Polymers*, *20*, 291–299.
- Aymard, P., Martin, D. R., Plucknett, K., Foster, T. J., Clark, A. H., & Norton, I. T. (2001). Influence of thermal history on the structural and mechanical properties of agarose gels. *Biopolymers*, *59*, 131–144.
- Burrow, T. R. (2005). Recent Advances In Chemically Treated Lyocell Fibres. *Lenzinger Berichte*, *84*, 110–115.
- Cairns, P., Miles, M. J., & Morris, V. J. (1986). Intermolecular binding of xanthan gum and carob gum. *Nature*, *322*, 89–90.
- Cairns, P., Miles, M. J., Morris, V. J., & Brownsey, G. J. (1987). X-Ray fibre diffraction studied of synergistic, binary polysaccharide gels. *Carbohydrate Research*, *160*, 411–423.
- Chanliaud, E., Burrows, K. M., Jeronimidis, G., & Gidley, M. J. (2002). Mechanical properties of primary plant cell wall analogues. *Planta*, *215*, 989–996. <https://doi.org/10.1007/s00425-002-0783-8>.
- Chanzy, H., Dubé, M., & Marchessault, R. H. (1978). Shish-kebab morphology. Oriented recrystallization of mannan on cellulose. *Technical Association of the Pulp and Paper*

- Industry, 61(7), 81–82.
- Chanzy, H. D., Grosrenaud, A., Joseleau, J. P., Dubé, M., & Marchessault, R. H. (1982). Crystallization behavior of glucomannan. *Biopolymers*, 21, 301–319.
- Chumnanklang, R., Panyathanmaporn, T., Sittiseripratip, K., & Suwanprateeb, J. (2007). 3D printing of hydroxyapatite: Effect of binder concentration in pre-coated particle on part strength. *Material Science and Engineering C: Materials for Biological Applications*, 27, 914–921. <https://doi.org/10.1016/j.msec.2006.11.004>.
- Cui, S. W., & Roberts, K. T. (2009). Dietary fiber: Fulfilling the promise of added-value formulations. In S. Kasapis, I. Norton, & J. Ubbink (Eds.). *Modern biopolymer science - Bridging the divide between fundamental treatise and industrial application* (pp. 399–448). Oxford: Academic Press.
- Cuq, B., Mandato, S., Supagro, M., Jeantet, R., Ouest, A., Saleh, K., De, U. T., Ruiz, T., & Montpellier, U. (2013). Agglomeration/Granulation in food powder production. In B. Bhandari, N. Bansal, M. Zhang, & P. Schuck (Eds.). *Handbook of food powders: Processes and properties* (pp. 150–177). Woodhead Publishing Limited. <https://doi.org/10.1533/9780857098672.1.150>.
- Dea, I. C. M., & Rees, D. A. (1987). Affinity interactions between agarose and  $\beta$ -1,4-glycans: A model for polysaccharide associations in algal cell walls. *Carbohydrate Polymers*, 7, 183–224.
- Dea, I. C. M., Clark, A. H., & McCleary, B. V. (1986). Effect of the molecular structure of galactomannans and their interaction properties – the role of unsubstituted sides. *Food Hydrocolloids*, 1, 129–140.
- Derby, B. (2010). Inkjet printing of functional and structural materials: Fluid property requirements, feature stability, and resolution. *Annual Review of Materials Research*, 40, 395–414.
- Derossi, A., Caporizzi, R., Azzollini, D., & Severini, C. (2017). Application of 3D printing for customized food. A case on the development of a fruit-based snack for children. *Journal of Food Engineering*, 1–11.
- Diaz, J. V., Noort, M. W. J., Van Bommel, K. J. C. (2017). Method for the production of an edible object by powder bed (3D) printing and food products obtainable therewith. United States Patent. US 20170164650 A1.
- Doyle, J. P., Lyons, G., & Morris, E. R. (2009). New proposals on “hyperentanglement” of galactomannans: Solution viscosity of fenugreek gum under neutral and alkaline conditions. *Food Hydrocolloids*, 23, 1501–1510.
- García-Ochoa, F., Santos, V. E., Casas, J. A., & Gomez, E. (2000). Xanthan gum: Production, recovery, and properties. *Biotechnology Advances*, 18, 549–579. [https://doi.org/10.1016/S0734-9750\(00\)00050-1](https://doi.org/10.1016/S0734-9750(00)00050-1).
- Ghaffar, S. H. (2016). Straw fibre-based construction materials. In M. Fan, & F. Fu (Eds.). *Advanced High strength natural fibre composites in construction* (pp. 257–283). Woodhead Publishing Limited.
- Gibson, L. J. (2012). The hierarchical structure and mechanics of plant materials. *Journal of the Royal Society, Interface*, 9(76), 2749–2766.
- Goda, K., & Sreekala, M. S. (2006). Improvement of plant based natural fibers for toughening green composites — Effect of load application during mercerization of ramie fibers. *Composites A: Applied Science and Manufacturing*, 37(12), 2213–2220.
- Godoi, F. C., Prakash, S., & Bhandari, B. R. (2016). 3d printing technologies applied for food design: Status and prospects. *Journal of Food Engineering*, 179, 44–54.
- Goycoolea, F. M., Morris, E. R., & Gidley, M. J. (1995). Viscosity of galactomannans at alkaline and neutral pH: evidence of ‘hyperentanglement’ in solution. *Carbohydrate Polymers*, 27, 69–71.
- Goycoolea, F. M., Richardson, R. K., Morris, E. R., & Gidley, M. J. (1995). Stoichiometry and conformation of xanthan in synergistic gelation with locust bean gum or Konjac Glucomannan: evidence for heterotypic binding. *Macromolecules*, 28, 8308–8320.
- Hajji, F., Mitchell, J. R., & Foster, T. J. (2011). Relationship between the conformational structure and processability of hydrocolloids. *Gums and stabilisers for the food industry* 67–76.
- Hermans, P. H., & Weidinger, A. (1946). On the recrystallization of amorphous cellulose. *Journal of the American Chemical Society*, 68, 2547–2552.
- Hess, K., Kiessig, H., & Gunderman, J. Z. (1941). *Physik. Chem*, B49, 64.
- Holland, S., Foster, T., MacNaughtan, W., & Tuck, C. (2018). Design and characterisation of food grade powders and inks for microstructure control using 3D printing. *Journal of Food Engineering*, 220, 12–19.
- Ju, X., Bowden, M., Brown, E. E., & Zhang, X. (2015). An improved X-ray diffraction method for cellulose crystallinity measurement. *Carbohydrate Polymers*, 123, 476–481. <https://doi.org/10.1016/j.carbpol.2014.12.071>.
- Kipphan, H. (2001). *Fundamentals. Handbook of print media: Technologies and production methods*. Springer Science & Business Media.
- Klemm, D., Schmauder, H., & Heinze, T. (2002). *Cellulose. Biopolymers. Vol. 6 polysaccharides II polysaccharides from eukaryotes*. 275–287.
- Lanaro, M., Forrestal, D. P., Scheurer, S., Slinger, D. J., Liao, S., Powell, S. K., et al. (2017). 3D printing complex chocolate objects: Platform design, optimization and evaluation. *Journal of Food Engineering*, 215, 13–22.
- Lipton, J. I. (2017). Printable food: The technology and its application in human health. *Current Opinion in Biotechnology*, 44, 198–201.
- Millen, C., Gupta, G., Sen, & Archer, R. (2012). Investigations into colour distribution for voxel deposition in 3D food formation. *International Conference on Control, Automation and Information Sciences* (pp. 202–207).
- Morris, E. R., Rees, D. A., Young, G., Walkinshaw, M. D., & Darke, A. (1977). Order-disorder transition for a bacterial polysaccharide in solution. A role for polysaccharide conformation in recognition between *Xanthomonas* pathogen and its plant host. *Journal of Molecular Biology*, 110(1), 1–16.
- Ong, E. E. D., O’Byrne, S., & Liow, J. (2018). *Molecular dynamics study on the structural and dynamic properties of xanthan gum in a dilute solution under the effect of temperature*. AIP Conference Proceedings 1954 030008.
- Oskay, W. (2007). *Solid Freeform Fabrication: DIY, on the cheap, and made of pure sugar*. [online] Available at: . [Accessed: 12 August 2015] <http://www.evilmadscientist.com/2007/solid-freeform-fabrication-diy-on-the-cheap-and-made-of-pure-sugar/>.
- Paes, S. S., Sun, S., MacNaughtan, W., Ibbett, R., Ganster, J., Foster, T. J., et al. (2010). The glass transition and crystallization of ball milled cellulose. *Cellulose*, 17, 693–709.
- Pallottino, F., Hakola, L., Costa, C., Antonucci, F., Figorilli, S., & Seisto, A. (2016). Printing on food or food printing : A review. *Food and Bioprocess Technology*, 9(5), 725–733. <https://doi.org/10.1007/s11947-016-1692-3>.
- Park, S., Baker, J. O., Himmel, M. E., Parilla, P. A., & Johnson, D. K. (2010). Cellulose crystallinity index: measurement techniques and their impact on interpreting cellulase performance. *Biotechnology for Biofuels*, 3. <https://doi.org/10.1186/1754-6834-3-10>.
- Public Health England (2015). *Guidelines on reducing sugar in food published for industry*. [press release]. 30 March. Available at: . (Accessed: 25 July 2017) <https://www.gov.uk/government/news/guidelines-on-reducing-sugar-in-food-published-for-industry>.
- Rasband, W.S. (2018) ImageJ User Guide. U.S. National Institutes of Health, Bethesda, Maryland, USA. <https://imagej.nih.gov/ij/docs/guide/146-30.html>. 1997-2016.
- Rosenau, T., Potthast, A., Sixta, H., & Kosma, P. (2001). The chemistry of side reactions and byproduct formation in the system NMMO/cellulose (Lyocell process). *Progress in Polymer Science*, 26, 1763–1837.
- Schindelin, J., Arganda-Carreras, I., Frise, E., Kaynig, V., Longair, M., Pietzsch, T., et al. (2012). Fiji: An open-source platform for biological-image analysis. *Nature Methods*, 9(7), 676–682.
- Schmutzler, C., Zimmermann, A., & Zaeh, M. F. (2016). Compensating warpage of 3D printed parts using free-form deformation. *Proceedings of 48th CIRP Conference on MANUFACTURING SYSTEMS - CIRP CMS 2015*, 41, 1017–1022.
- Sol, E. J., Van Der Linden, D., & Van Bommel, K. J. C. (2015). *3D food printing: The barilla collaboration*. [online] Available at: . [Accessed: 11 August 2015] <https://ec.europa.eu/jrc/sites/jrcsh/files/20150225-presentation-jan-sol.pdf>.
- Southerland, D., Walters, P., & Huson, D. (2011). Edible 3D printing, in proceeding of NIP & digital fabrication conference. *Society for Imaging Science and Technology*, 2, 819–822.
- Sozer, N., Lille, M., Nurmela, A., Nordlund, E., & Mets, S. (2018). Applicability of protein and fiber-rich food materials in extrusion-based 3D printing. *Journal of Food Engineering*, 220, 20–27.
- Stephen, A. M., Phillips, G. O., & Williams, P. A. (2006). *Food polysaccharides and their applications* (2nd ed.). Taylor and Francis.
- Sun, J., Zhou, W., Yan, L., Huang, D., & Lin, L. (2018). Extrusion-based food printing for digitalized food design and nutrition control. *Journal of Food Engineering*, 220, 1–11.
- Vancauwenbergh, V., Katalagianakis, L., Wang, Z., Meerts, M., Hertog, M., Verboven, P., Moldenaers, P., Hendrickx, M. E., Lammertyn, J., & Nicola, B. (2017). Pectin based food-ink formulations for 3-D printing of customizable porous food simulants. *Innovative Food Science & Emerging Technologies*, 42, 138–150.
- Von Hasseln, K., Von Hasseln, E. M., Williams, D. X. (2014). Apparatus and Method for Producing a Three-Dimensional Food Product. 3D Systems Inc. United States Patent US 2014/0154378 A1.
- Wegrzyn, T. F., Golding, M., & Archer, R. H. (2012). Food Layered Manufacture: A new process for constructing solid foods. *Trends in Food Science & Technology*, 27, 66–72.
- Whitney, S. E., Brigham, J. E., Darke, A. H., Reid, J. S., & Gidley, M. J. (1998). Structural aspects of the interaction of mannan-based polysaccharides with bacterial cellulose. *Carbohydrate Research*, 307, 299–309.
- Winkworth-Smith, C. G. (2014). *Cellulose composite structures – By design*. Unpublished PhD thesis. University of Nottingham.
- Wüstenberg, T. (2014). *Cellulose and cellulose derivatives in the food industry: Fundamentals and applications*. United Kingdom: John Wiley and Sons Ltd.
- Yang, J., Wu, L., Liu, J. (2000). Method for Rapidly Making a 3D Food Object. US Patent US2680784 B1.